CHIN. PHYS. LETT. Vol. 38, No. 3 (2021) 035202 Review

Energetic Particle Physics on the HL-2A Tokamak: A Review

Pei-Wan Shi(施培万)[1,2], Wei Chen(陈伟)[1*], and Xu-Ru Duan(段旭如)[1]

[1]*Southwestern Institute of Physics, Chengdu 610041, China*
[2]*Key Laboratory of Materials Modification by Laser, Ion, and Electron Beams (Ministry of Education), School of Physics, Dalian University of Technology, Dalian 116024, China*

(Received 27 November 2020; accepted 5 February 2021; published online 2 March 2021)

Interaction between shear Alfvén wave (SAW) and energetic particles (EPs) is one of major concerns in magnetically confined plasmas since it may lead to excitation of toroidal symmetry breaking collective instabilities, thus enhances loss of EPs and degrades plasma confinement. In the last few years, Alfvénic zoology has been constructed on HL-2A tokamak and series of EPs driven instabilities, such as toroidal Alfvén eigenmodes (TAEs), revered shear Alfvén eigenmodes (RSAEs), beta induced Alfvén eigenmodes (BAEs), Alfvénic ion temperature gradient (AITG) modes and fishbone modes, have been observed and investigated. Those Alfvénic fluctuations show frequency chirping behaviors through nonlinear wave-particle route, and contribute to generation of axisymmetric modes by nonlinear wave-wave resonance in the presence of strong tearing modes. It is proved that the plasma confinement is affected by Alfvénic activities from multiple aspects. The RSAEs resonate with thermal ions, and this results in an energy diffusive transport process while the nonlinear mode coupling between core-localized TAEs and tearing modes trigger avalanche electron heat transport events. Effective measures have been taken to control SAW fluctuations and the fishbone activities are suppressed by electron cyclotron resonance heating. Those experimental results will not only contribute to better understandings of energetic particles physics, but also provide technology bases for active control of Alfvénic modes on International Thermonuclear Experimental Reactor (ITER) and Chinese Fusion Engineering Testing Reactor (CFETR).

DOI: 10.1088/0256-307X/38/3/035202

1. Introduction. Energetic particles (EPs), including α particle, fast ion and fast electron, originate from fusion reactions or external auxiliary heating, and play important roles in burning plasmas. The slowdown of EPs due to Coulomb collisions with thermal particles benefit plasma self-heating, and good confinements of EPs are necessary for achieving high fusion gain. The EPs are regarded as mediators of cross-scale coupling, and intermediate between microscopic Larmor radius and macroscopic plasma equilibrium scale lengths.[1] Those particles can drive macro- and meso-scales instabilities through interacting with shear Alfvén wave. Amount of Alfvénic modes, i.e., eigenmodes and energetic particle modes, have been predicted and confirmed in both theoretical and experimental frames.[2,3] The instabilities play a negative or a positive role in the performance of fusion plasmas. On the one hand, the SAWs fluctuation is generally recognized to downgrade energetic particle confinement by inducing anomalous transports and causing substantial loss with different physical mechanisms.[4–7] The electromagnetic instability affects thermal particles confinement as well.[8,9] It is found that overlapping modes resonantly couple to bulk thermal electrons, then cause stochastic diffusion and finally lead to electron temperature flattening in the core.[10,11] On the other hand, EPs driven instabilities can be treated as kinetic spectroscopies to monitor dynamic evolution of equilibrium parameters,[12] or as energy channel,[13,14] which contributes to sustain a steady state internal transport barrier and to optimize plasma confinement.[15,16] To effectively avoid potential threats of Alfvénic events and to improve EPs confinement properties, more attention should be paid to the underlying mechanisms of excitation, saturation and damping through experimental verification associated with numerical simulations and analytical theory. With development of external auxiliary heating technology and multiple plasma diagnostics, the zoology of Alfvénic instabilities has also been found on HL-2A tokamak. In this article, an overview of energetic particle driven instabilities in toroidal plasma will be given. The heating system and plasma diagnostics are firstly presented. Then, experimental observations and confirmations of Alfvénic activities driven by fast ions or electrons are reviewed in Section 3. Nonlinear activities induced by nonlinear wave-particle and wave-wave interaction are exhibited in Section 4. Attentions are mainly devoted to nonlinear coupling between Alfvénic modes and tearing mode. Effects of EPs driven instabilities on energetic and thermal particle confinements will be discussed in Section 5, and the suppression technique based on ECRH is arranged in Section 6. A summary

Supported by the National Key R&D Program of China (Grant Nos. 2019YFE03020000 and 2017YFE0301200), the National Natural Science Foundation of China (Grant Nos. 11835010, 11875021 and 11875024), and the China Postdoctoral Science Foundation (Grant No. 2020M670756).
*Corresponding author. Email: chenw@swip.ac.cn
© 2021 Chinese Physical Society and IOP Publishing Ltd

of relevant issues in this work and the next experimental schedules on HL-2A/2M are given finally.

2. Auxiliary Heating Systems and Plasma Diagnostics. HL-2A is a medium-size tokamak with predominantly circular cross-section and major/minor radius of $R/a = 1.65\,\mathrm{m}/0.4\,\mathrm{m}$. The device is developed for scientific researches related to advanced tokamak physical experiments, technical and engineering issues of ITER or fusion reactor, and it can operate at limiter or divertor configuration with plasma current $I_\mathrm{p} = 100$–$350\,\mathrm{kA}$, toroidal magnetic field $B_\mathrm{t} = 1.0$–$1.8\,\mathrm{T}$ and line average electron density $\overline{n_\mathrm{e}} = (0.4\text{–}5)\times10^{19}\,\mathrm{m}^{-3}$. Further, the HL-2A is equipped with neutral beam injection (NBI), low-hybrid wave/current drive (LHCD) and electron cyclotron resonance heating/electron cyclotron current drive (ECRH/ECCD) systems. The NBI system consists of two independent beamlines and is the main source of fast ions in present HL-2A plasma. Both of beamlines are tangentially injected with angles of 58° and can achieve maximum port-through power of 1.2 MW/1.0 MW and accelerated particle energy of 50 keV/42 keV. More detailed parameters for the beamlines are given in Table 1. There are 6 sets of ECRH/ECCD systems with 68 GHz/0.5 MW/1 s and 2 sets with 140 (105) GHz/1 MW/3 s on the HL-2A tokamak. High power O-mode or X-mode microwaves are injected into plasma from low field side. The well designed steerable plane mirrors can change the injection angle in the range from 0° to ±30° and enable current drive with the same or different directions from plasma current. The LHCD power coupling is optimized using passive active multi-junction antenna, by which the coupled power reaches 1.4 MW in high confinement regime (H-mode).

Those auxiliary heating systems give raise to energetic particles in plasma while multiple advanced diagnostics, as arranged in Fig. 1, monitor dynamic evolutions of energetic particles and SAWs fluctuation. The Mirnov coils consist of poloidal (10 probes at low field side and 8 probes at high field sides) and toroidal (10 probes) arrays. It is a powerful tool for direct measurement of electromagnetic turbulence. There are 32 channels for charge exchange recombination spectroscopy (CXRS),[17] which can achieve spacial/temporal resolution of 1 cm/12.5 ms and provide information for ion temperature and toroidal rotation frequency. The electron cyclotron emission (ECE) radiometer[18] and Thomson scattering system contribute to electron temperature profile measurement. The FIR laser interferometer and frequency modulated-continuous wave (FMCW) reflectometer[19] are developed for exploring electron density while the microwave interferometer,[20] multichannel reflectometer[21] [working as conventional or Doppler backward scattering (DBS) reflectometer] and beam emission spectroscopy (BES) for electron density fluctuation. The soft x-ray arrays and electron cyclotron emission imaging (ECEI)[22] with 8 (radial)×24(vertical) = 192 channels enable visual observations of magnetohydrodynamic instability. Recently, energetic particle diagnostics,[23] such as fast ion deuterium Alpha (FIDA), fast ion loss probe, neutron detector and Cadmium-telluride (CdTe) detectors, have also been installed. Those diagnostics offer valuable information during experimental campaign aiming at Alfvénic activities. Noted that, several numeral codes, i.e., EFIT, tokamak simulation code and current profile fitting code, have been introduced or developed to calculate safety factor and plasma pressure profiles, which are crucial for explanations of EPs driven instabilities.

Table 1. Parameters of two neutral beamlines on HL-2A.

Parameters	1st beamline	2nd beamline
Maximum port-through power	1.2 MW	1.0 MW
Accelerated particle energy	50 keV	42 keV
Neutralization efficiency	70%	70%
Extracted beam current	24 A	16 A
Number of ion sources	4	4
Injected angle	58°	58°
Injected gas	H_2 and D_2	H_2 and D_2

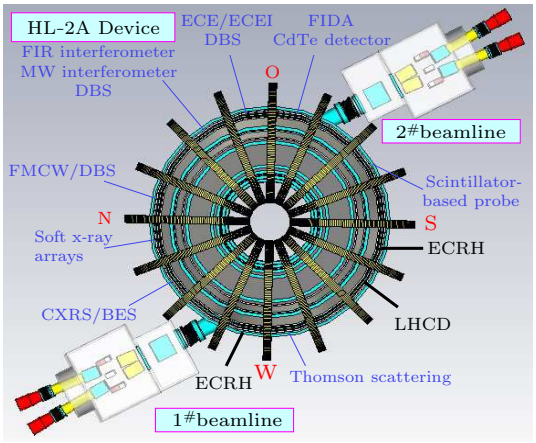

Fig. 1. Arrangements of auxiliary heating systems and main diagnostics for energetic particle experiments on HL-2A tokamak.

3. Experimental Observations and Confirmations. The generalized fishbone-like dispersion relation (GFLDR),[24] given by $i\Lambda = \delta W_f + \delta W_k$, suggests that there mainly are two types of energetic particle driven modes, i.e., Alfvén eigenmodes with $\mathrm{Re}\Lambda^2 < 0$ and energetic particle modes with $\mathrm{Re}\Lambda^2 > 0$ (here, δW_f and δW_k come from fluid magnetohydrodynamics and energetic particle contributions in the regular ideal regions, while $i\Lambda$ is the inertial layer contribution due to thermal ions). The former is located at the shear Alfvén frequency gap due to different physical effects and easily driven by fast ions or electrons. The latter interacts with continuum and can be excited when the wave-particle power exchanged with energetic particles is high enough to exceed continuum damping. The two kinds of instabilities have already been found on HL-2A.

3.1. Toroidal and Reversed Shear Alfvén Eigenmodes. As the most famous discrete SAW spectrum in magnetic confined fusion devices, toroidal Alfvén eigenmodes (TAEs) are firstly predicted in theory[25] and then confirmed by experiments on TFTR.[26] The TAEs are thought of as the most danger Alfvén eigenmodes due to spacial overlapped global mode structures, which may enhance energy or particle transports. The modes have been observed in high density discharges on HL-2A tokamak.[27] The Alfvénic fluctuations are driven by sub-Alfvénic fast ions and possess ballooning mode structures, i.e., mode amplitudes are stronger in low field side than that in high field side. The frequencies are proportional to Alfvén velocity and range about 120–180 kHz, which are approximatively half of Alfvén frequency. Statistical results reveal that the most unstable mode numbers are $n = 2$–3 and agree well with the theoretical prediction[28–30] given by $n_{\rm theory} = 1.2a\Omega_{\rm c}/(q^2 V_{\rm A})$, where $\Omega_{\rm c}$ is the fast ion cyclotron frequency, q is the safety factor and $V_{\rm A}$ is the Alfvén velocity. The TAEs can also be excited by energetic electrons during high power electron cyclotron resonant heating.[31] In this cases, the mode frequencies are higher than that in NBI heated plasma and profiles of energetic electrons are proved to play an important role in evolution of TAEs.[32]

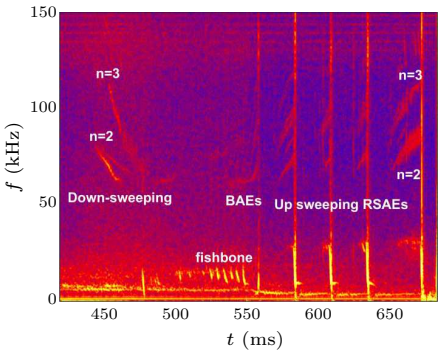

Fig. 2. Down sweeping RSAEs during plasma current ramp-up phase and up sweeping RSAEs before the sawtooth collapse. Reproduced with permission from Ref. [33]. Copyright 2014 IAEA Vienna.

Reversed shear Alfvén eigenmode (RSAE) is one of typical core localized electromagnetic instabilities in reverse magnetic shear plasma and characterized by frequency sweeping slowly due to slight change of minimum safety factors.[34] As $q_{\rm min}(t)$ changes during the discharge, RSAE frequency alters at a rate $\frac{d}{dt}\omega_{\rm RSAE}(t) \simeq \pm m\frac{V_{\rm A}}{R}\frac{d}{dt}q_{\rm min}(t)$. Here, plus and minus indicate the mode frequency sweep downward and upward, respectively. It makes RSAEs to be served as kinetic Alfvénic spectroscopy to monitor the $q_{\rm min}(t)$ evolution in experiment.[35,36] Both down-sweeping and up-sweeping RSAEs have been observed on HL-2A,[33] as shown in Fig. 2. The former is characterized by frequency down-sweeping when $q_{\rm min}$ decreases due to $q_{\rm min} > 1$ and $nq_{\rm min} - m > 0$ during plasma current ramp-up phase. The latter sweeps up with a drop of $q_{\rm min}$, owing to $q_{\rm min} < 1$ and $nq_{\rm min} - m < 0$ before sawtooth crash. Kinetic Alfvén eigenmode code analysis suggests that the down-sweeping modes are kinetic RSAEs and the up-sweeping modes are RSAEs. Excitation mechanism of two RSAEs are quite different. The preferred upward direction of RSAEs sweeping indicates that a Schrödinger type equation has a radial potential well, as opposed to a potential hill for the downward sweeping perturbations.[37] Hybrid simulation based on experimental parameters indicate that both of RSAEs are mainly driven by co-passing fast ions, but the fast ion beta is higher for excitation of down-sweeping RSAEs than that of up-sweeping modes.[38] Moreover, a group of slowly down-sweeping frequency coherent modes with $n = 3$–7 are often observed with an increase in edge safety factor. Those modes are characterized by multiple bands of modes with mean frequency decreasing steadily in time. The frequencies are much higher than that of traditional RSAEs and in the range $100 < f < 500$ kHz with $f_{\rm min} \sim f_{\rm TAE}$. The RSAE-like modes locate inside high order Alfvénic eigenmode gap of continuum, and the eigenfrequency or eigenfunction is determined by $q_{\rm min}$ and safety factor profile. Preliminary results suggest that there is a close relationship between the high frequency modes and internal transport barrier (ITB). However, evidences for the sweeping modes are quite limited and more experiments should be designed for the corresponding researches.

3.2. Beta Induced Alfvén Eigenmodes. Beta induced Alfvén eigenmodes (BAEs) are low-frequency Alfvén eigenmodes and locate in the continuum gap due to finite plasma beta. The modes can be excited by energetic ions, energetic electron as well as magnetic islands, which are labeled as i-BAE, e-BAE and m-BAE, respectively. The i-BAEs were firstly observed and found to cause large losses of fast ions on DIII-D.[39] Those modes are also driven in the HL-2A plasma.[40] The mode frequencies are around 60–95 kHz and the radial structures have been detected by a multi-channel microwave reflectometer. It is spectrum of microwave reflectometer with frequency of 40 GHz in Fig. 3(a), and Fig. 3(b) shows the two-dimensional density fluctuations filtered by numerical pass-band filter with frequency of 90–95 kHz. Noted that the cutoff layers of 34–40 GHz microwave are determined with the density profile measured by an FMCW reflectometer. The BAEs are highly localized at normalized radius of $\rho = 0.07$–0.26, which agrees with the numeral calculation. Furthermore, the experimental observations are well explained by GFLDR. There may be an electron density threshold for BAE excitation since the modes cannot be observed when line-averaged density is higher than $1.2 \times 10^{19}\,{\rm m}^{-3}$, where the modes may suffer from stronger ion landau damping.

The BAEs triggered by energetic electrons and the modes during presence of tearing mode activities have also captured great attentions. The e-BAEs are firstly confirmed on HL-2A[41] and they can be excited in

both Ohmic and electron cyclotron resonance heating plasma, as shown in Fig. 4. The mode frequency ranges from 10 kHz to 30 kHz, which is comparable to that of continuum accumulation point of the lowest frequency gap induced by shear Alfvén continuous spectrum due to finite beta effect. The e-BAEs are driven by barely circulating or deeply trapped particles, and are closely related to the population, energy and pitch angles of energetic electrons. The m-BAEs appear in pairs during appearance of strong tearing mode.[42,43] Two m-BAEs propagate in different diamagnetic drift directions and the mode numbers are $m/n = 2/1$ and $-2/-1$. Here, plus or minus represents the mode propagates in ion or electron diamagnetic drift direction. Frequency difference between the two modes is twice the fundamental frequency of tearing mode. It is worth pointing out that frequency of m-BAEs linearly depends on island width[44] and m-BAEs can be driven only when the magnetic islands width exceeds a threshold, which is about 3.4 cm on HL-2A.

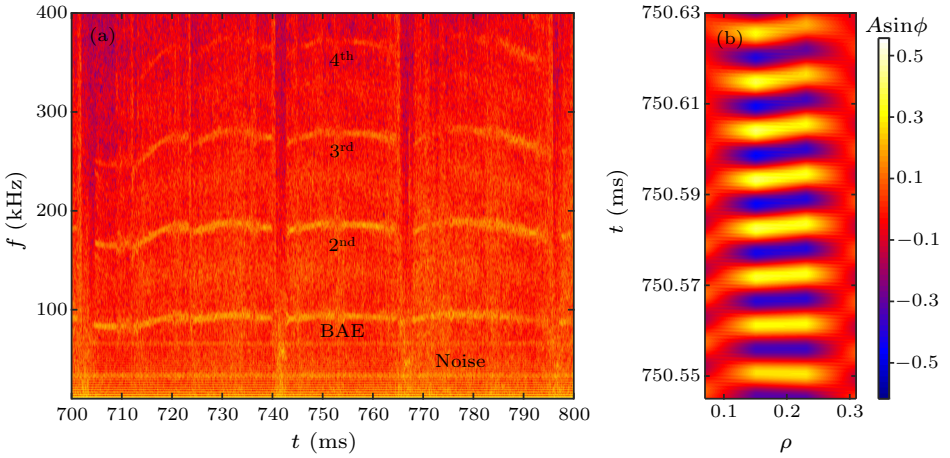

Fig. 3. (a) Beta induced Alfvén eigenmode and its multiple harmonics obtained from a multi-channel microwave reflectometer. (b) Radial mode structure of BAE in form of two-dimensional electron density fluctuation. Reproduced with permission from Ref. [40]. Copyright 2019 IAEA Vienna.

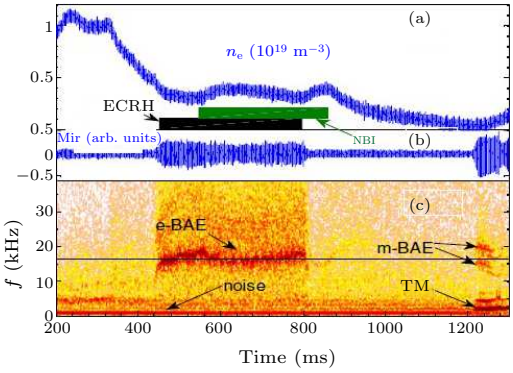

Fig. 4. History evolution of (a) central line-average density, (b) magnetic probe signal, (c) the spectrogram of magnetic probe signal in the presence of e-BAE. Reproduced with permission from Ref. [41]. Copyright 2010 by the American Physical Society.

3.3. KBM and AITG. The shear Alfvén acoustic continuum structure can be modified by diamagnetic drift effects with strong density and temperature gradients, so that there is a transition from BAE branch to small-scale kinetic ballooning mode (KBM) branch.[45] KBMs are usually driven by plasma pressure gradient and belongs to energetic particle mode family because its frequency depends strongly on properties of EPs.[46] The resistive kinetic ballooning modes on HL-2A are characterized by appearing with multiple harmonics and unchanged mode frequencies,[47] as shown in Fig. 5. The modes can not only cause a drop of neutron counts by deteriorating the confinement of energetic ions, but also affect bulk plasma performance via leading to Beta partial collapse and bulk plasma disruption. Generally, the maximum plasma beta in tokamaks can not exceed the Troyon limit which is predicted by ideal MHD kink-ballooning instability theory. Thus, KBMs may be treated as a precursor for the control of bulk plasma disruption. The experimental observations are well explained by GFLDR, which claims that real frequencies calculated with experimental inputs meet with typical KBM frequency ranges, i.e., $\omega_{*\mathrm{ip}}/2 < \omega_\mathrm{r} < \omega_{*\mathrm{ip}}$. Further, $\Omega_{*\mathrm{ip}} = \omega_{*\mathrm{ip}}/\omega_{\mathrm{ti}} \simeq 2 > \sqrt{7/4+\tau q} \simeq 1.58$ suggests that diamagnetic effect plays a crucial role in the plasma, where KBMs bench would be dominant. Here, $\omega_{\mathrm{ti}} = \sqrt{2T_\mathrm{i}/m_\mathrm{i}}/qR$ is ion transit frequency, $\omega_{*\mathrm{ip}}$ is ion diamagnetic frequency, $\omega_{*\mathrm{ip}} = \omega_{*\mathrm{ni}} + \omega_{*\mathrm{Ti}} = (T_\mathrm{i}/eB)k_\theta(\nabla \ln n_\mathrm{i})(1+\eta_\mathrm{i})$, $\eta_\mathrm{i} = \nabla \ln T_\mathrm{i}/\nabla \ln n_\mathrm{i}$ (the ion density $n_\mathrm{i} \simeq n_\mathrm{e}$), $\omega_{*\mathrm{ni}} = (cT_\mathrm{i}/eB_\mathrm{t})(\boldsymbol{k}\times\boldsymbol{b})\cdot\nabla \ln n_\mathrm{i}$, $\omega_{*\mathrm{Ti}} = (cT_\mathrm{i}/eB_\mathrm{t})(\boldsymbol{k}\times\boldsymbol{b})\cdot\nabla \ln T_\mathrm{i}$ and ω_A is the Alfvén frequency.

Theoretical prediction indicates that finite ∇T_i effects give rise to Alfvénic ion temperature gradient (AITG) mode due to wave-particle interactions with thermal ions via geodesic curvature coupling.[48–50] It is a new branch connecting KBM (diamagnetic effects $\Omega_{*\mathrm{ip}} \gg \sqrt{7/4+\tau q}$) and BAE (ion compression effects $\Omega_{*\mathrm{ip}} \ll \sqrt{7/4+\tau q}$), and becomes most un-

stable when the condition $\Omega_{*\mathrm{ip}} \sim \sqrt{7/4+\tau}q$ is fulfilled. Figure 6 gives a typical example of AITG instability in the neutral beam heated plasma on HL-2A Tokamak.[51] The left column shows discharge parameters, including plasma current, line-averaged electron density, power of heating and ions temperatures, while the right part presents spectrum of microwave interferometer and soft x-ray signals. Several groups of high frequency coherent modes are unstable in plasmas with weak shear and low pressure gradients. The frequencies range $\omega_{\mathrm{BAE}} < \omega < \omega_{\mathrm{TAE}}$ and the toroidal mode numbers are $n = 2$–8. The instability can translate to or appear together with low frequency fishbone modes or long lived modes. The interaction between AITG activity and energetic particles needs to be investigated further, since these instabilities may link with formation of ITB by energetic particles via generation of zonal field structures.[1] Those modes can be triggered not only in NBI heating cases, but also in Ohmic plasma, where the time trace of fluctuation spectrogram can be either a frequency staircase with different modes excited at different times or multiple modes simultaneously coexisting.[52]

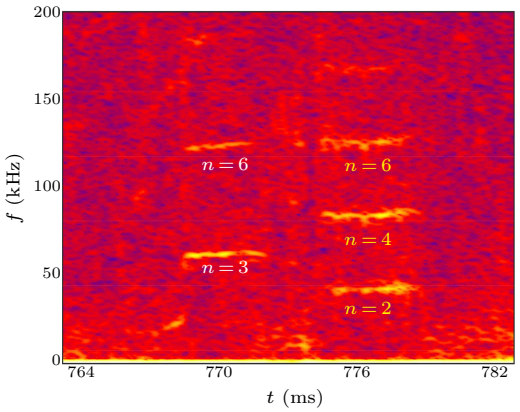

Fig. 5. Kinetic ballooning modes in the neutral beam heated plasma. Reproduced with permission from Ref. [47]. Copyright 2016 IAEA Vienna.

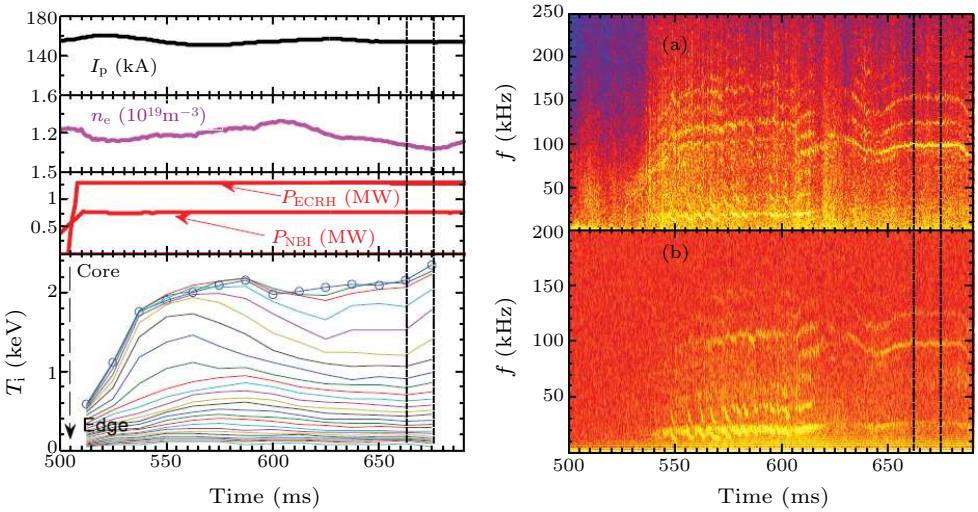

Fig. 6. Analyzing the reference discharge with Alfvénic ion temperature gradient modes. Left column: plasma current, line-averaged electron density, heating power and ion temperature. Right column: spectrograms of the core microwave interferometer (a) and soft x-ray (b) signals. Reproduced with permission from Ref. [51]. Copyright 2018 IAEA Vienna.

3.4. Fishbone Modes. Fishbone modes are the most unstable energetic particle modes on HL-2A tokamak and excited by energetic ions or energetic electrons, marked as i-fishbone and e-fishbone, respectively. The i-fishbones can be divided into three categories depending on their frequency evolutions.[53] Firstly, hybrid sawtooth-fishbone appears during the whole of sawtooth ramp and it can easily be distinguished from precursor oscillations, because the mode frequency is usually higher than that of sawtooth precursor. Then, it is the classical fishbone mode with frequency decreasing remarkably during its burst. Mode amplitude reaches the maximum when frequency sweeps down completely, then it decreases continuously until the mode vanishes. Finally, it is the semi-continuous $m/n = 1/1$ activity, i.e., the so-called run-on fishbone. The mode does not show a quickly sweeping in frequency and its amplitude exhibit bursting behavior, which is different from the saturated amplitude of long-lived mode.[54]

Strong resonant and non-resonant e-fishbone modes can be observed in the ECRH+ECCD plasma. Here, 'resonant' derives from the existence of $q = 1$ resonant surface and 'non-resonant' originates from the absence of $q = 1$ surface ($q_{\mathrm{min}} > 1$). The resonant e-fishbone modes are excited by precessional movement of energetic trapped electrons and usually display similar evolution dynamics to the classical i-fishbone. Specially, periodic frequency jump phenomena may take place during high power ECRH injection,[55] as shown in Fig. 7. The soft x-ray tomography reveals that poloidal and toroidal mode numbers are $m/n = 1/1$ and $2/2$ for the lower and higher frequency fishbones. The frequencies of two modes in-

crease with ECRH power and there is a power threshold of 0.9 MW for the frequency jump phenomena. The non-resonant e-fishbone modes are driven on HL-2A tokamak with high power ECRH and co-ECCD.[56] The co-ECCD means driving direction of ECCD is the same to plasma current. Unlike resonant e-fishbone modes with periodic strong bursting amplitude and rapid chirping-down frequency, non-resonant modes always have saturated amplitudes and keeps for a long time, as shown in Fig. 8.

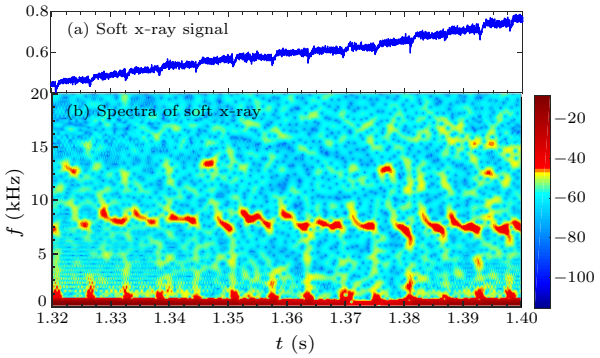

Fig. 7. Typical characteristics of frequency jump phenomena in shot 17892: (a) soft x-ray signal and (b) the frequency spectra. Reproduced with permission from Ref. [55]. Copyright 2013 IAEA Vienna.

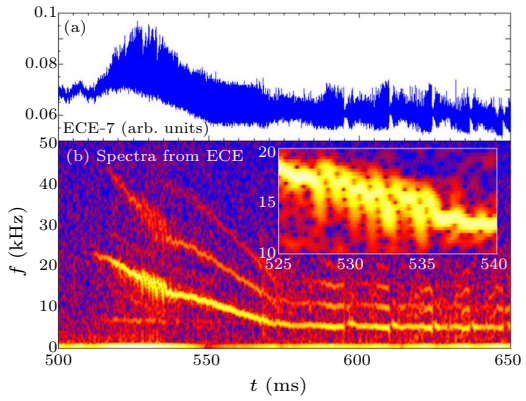

Fig. 8. Strong energetic electron induced non-resonant fishbone modes during on-axis high power ECRH + co-ECCD in shot 24067. (a) ECE signal with $r = 7.3$ cm (b) spectrogram of ECE signal. Reproduced with permission from Ref. [56]. Copyright 2017 IAEA Vienna.

However, there may be transitions between steady state nonlinear oscillations and moderate bursting pulsations for the non-resonant modes. It is similar to that driven by lower hybrid power injection on FTU.[57] No obvious differences between mode structures of two e-fishbone modes have been found by the ECEI system. Numerical analysis based on dispersion relationship of internal kink mode suggests that frequency behaviors of non-resonant e-fishbone are governed by safety factor. The modes are stable when $q_{\min}$ is larger than a certain value, and the frequency is proportional to $q_{\min}$ when $q_{\min}$ is larger than unity. With decreasing $q_{\min}$, the frequency drops while growth rate remains constant, which is in agreement with experimental observations.

3.5. The $m/n = 2/1$ Fishbone-Like Modes. The fishbone modes are usually generated from interaction between energetic particles and $m/n = 1/1$ internal kink modes. Recently, the $m/n = 2/1$ fishbone-like modes with amplitude-bursting/frequency-chirping phenomenons are firstly observed on HL-2A tokamak,[58,59] as given in Fig. 9. As the direct result of $m/n = 2/1$ tearing mode interacting with energetic ions, the modes occur only when tearing mode rotation direction changes from electron to ion diamagnetic drift. Mode frequencies chirp downward faster and amplitudes (dB_θ/dt) are much larger than that of $m/n = 1/1$ fishbone on HL-2A. Nonlinear hybrid kinetic-MHD simulations with M3D-K code suggest that co-passing fast ions are responsible for the drive of fishbone-like modes when wave-particle resonance condition of $\omega_\phi - 2\omega_\theta - \omega = 0$ is satisfied, where ω_ϕ and ω_θ are the toroidal and poloidal angular frequencies of energetic ions. Significant fast ions redistribution and losses are observed during simulation. The scaling of lost ions fraction with fluctuation amplitude arrives at $f_{\rm loss} \sim \sqrt{A_{\max}}$, indicating that the loss is convective. However, the loss process cannot be referred in experiment due to absences and limitations of energetic particle diagnostics.

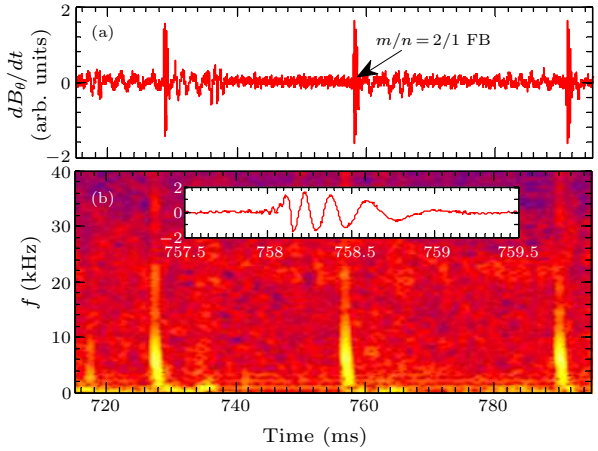

Fig. 9. The $m/n = 2/1$ fishbone modes detected by magnetic coil probe: (a) the raw signal and (b) corresponding spectrogram of magnetic probe signal and enlarged Mirnov signal during a burst. Reproduced with permission from Ref. [59]. Copyright 2020 IAEA Vienna.

4. Nonlinear Dynamic Evolutions of Alfvénic Modes. Nonlinear evolutions may determine the excitation and saturation of Alfvénic modes and it is one of most important topics in energetic particle physics. There are two routes for Alfvénic fluctuation nonlinear dynamic evolutions, i.e., wave-particle interactions and wave-wave interactions.[60] The former is described as single wave-particle phase space nonlinear dynamics dominated by resonant particles and can be explained in the bump-on-tail paradigm[61] or fishbone paradigm,[62,63] depending on the nonlinear wave-particle interaction induced frequency chirping rates. The latter describes nonlinear spectrum evolution due to nonlinear couplings among multi-

ple modes. It may take place via Compton scattering of bulk ions,[64] magnetohydrodynamic nonlinearity effects[65] and zonal structure generation.[66,67] In this section, attentions are devoted to the nonlinear activities of Alfvénic modes on HL-2A.

4.1. Frequency Down-Chirping and Pitch-Fork Splitting. Nonlinear wave-particle interaction usually results in frequency chirping activity. Two kinds of frequency chirping behaviors of Alfvénic modes, i.e., down-chirping and pitch-fork splitting, can be observed on HL-2A tokamak, as shown in Figs. 10(b) and 10(e). The two behaviors lead to magnetic fluctuation of $|B_\theta|_{\max} = 2\,\mu\mathrm{T}$ and $10\,\mu\mathrm{T}$ in Figs. 10(a) and 10(d), respectively. The growth rate of down-chirping mode can be estimated as $\gamma_{\exp} = \frac{d|B_\theta|}{dt}/|B_\theta|$ and it is $\gamma_{\exp} = 5\times10^3\,\mathrm{s}^{-1}$, where $|B_\theta|$ is the envelope of $B_\theta(t)$. Kinetic drive γ_l is approximated to intrinsic damping rate γ_d from background plasma for the pitch-fork splitting. Dependence of angular frequency on evolution time is predicted as $\omega = \omega_0 \pm \gamma_\mathrm{l}\sqrt{\gamma_\mathrm{d} t}$. The least square fitting has been performed, as shown in Fig. 10(f), based on frequencies picked up from experiments, the γ_l and γ_d are deduced as $\gamma_\mathrm{l} = \gamma_\mathrm{d} \sim 1.0\times10^4\,\mathrm{s}^{-1}$. The two nonlinear behaviors always exist alone, but can change into each other in given conditions. The frequency chirping behaviors are close to the dynamic evolutions of hole and clump pairs on phase space.[68] The hole leads to continuous upshift of mode frequency while the clump contributes to downshift movement. When the hole and clump pairs are broken, i.e., in the case that only hole or clump exists, Alfvénic modes will show mainly up-chirping or down-chirping features.[69] The connections between hole-clump pairs evolutions and frequency chirping processes have been experimentally notarized by neutral particle analyzer on LHD.[70] Actually, the Berk–Breizman model[71–73] provides quantitative analysis for the nonlinear wave-particle resonances. It claims that interactions among wave, energetic ions and collision effects may exhibit steady-state, periodic, chaotic and explosive regimes, depending on the evolutions of mode amplitudes. It has been utilized to analyze frequency chirping properties of Alfvén modes on HL-2A.[74] Moreover, a relay runner model[75] is also developed for the nonlinear evolutions of energetic particle modes and it provides a good interpretation for fast chirping modes that move radially while the frequencies are changing.

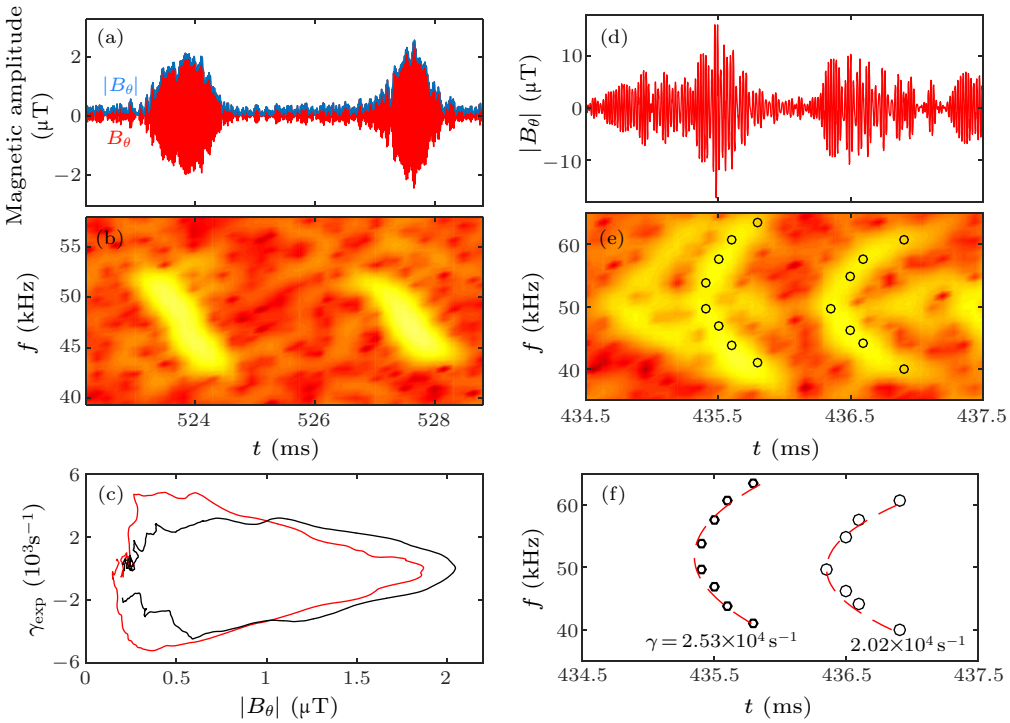

Fig. 10. (a) and (d) Magnetic fluctuations induced by Alfvénic modes; dynamic evolution of (b) frequency down-chirping and (e) pitch-fork splitting; (c) growth rates obtained from $\gamma_{\exp} = \frac{d|B_\theta|}{dt}/|B_\theta|$; (f) numerical fitting based on $\omega = \omega_0 \pm \gamma_\mathrm{l}\sqrt{\gamma_\mathrm{d} t}$

4.2. Nonlinear Coupling between Alfvénic Modes and Tearing Modes. Nonlinear behavior induced by wave-particle resonance is transient and periodic, in contrast, nonlinear coupling among Alfvénic modes (AMs) and tearing modes maintains for a long time and it will not come to an end until plasma collapse occurs.[76–78] The wave-wave interaction can produce different scale structures and determine their excitations, saturations or damping. It is responsible for the excitation of axisymmetric modes in ellipticity induced Alfvén eigenmode (EAE) frequency range on HL-2A.[79] Figure 11 presents frequency

spectrum with multiple modes during NBI heating. The AMs with toroidal mode numbers of $n_{\rm AMs} = 0, \pm1, \pm2, \pm3, 4$ and mode frequencies of $f_{\rm AMs}$(kHz) = 118.5, (128.5, 108.5), (138.5, 98.5), (148.5,88.5), 158.5, and an axisymmetric high frequency mode can be observed. Frequency and mode number differences of two adjacent AMs are comparable to the tearing mode frequency and toroidal mode number, i.e., $|f_{\rm AM_1} - f_{\rm AM_2}| = f_{\rm TM}$ and $|n_{\rm AM_1} - n_{\rm AM_2}| = n_{\rm TM}$, which indicates that there are nonlinear mode couplings between the AMs and tearing mode.

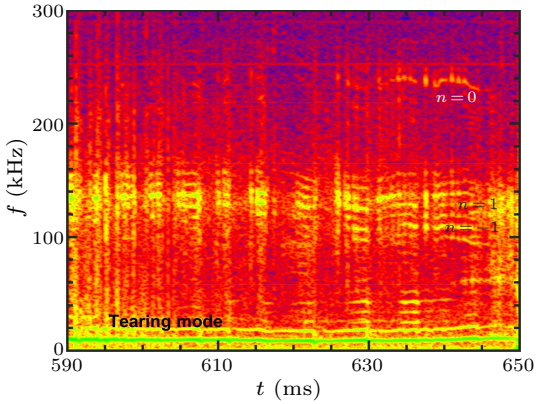

Fig. 11. Spectrogram of magnetic signal in low field side. Multiple modes coexist simultaneously in different frequency ranges and the toroidal mode numbers of $n = -1$, 0, 1 have been marked out.

To make the nonlinear process more visual, squared bicoherence is introduced as[80]

$$\hat{b}^2(f_1, f_2) = \frac{\langle |X_1(f_1)X_2(f_2)X_3^*(f_3)| \rangle}{\langle |X_1(f_1)X_2(f_2)|^2 \rangle \langle |X_3^*(f_3)|^2 \rangle}, \qquad (1)$$

with $f_1 \pm f_2 = f_3$ and $0 < \hat{b}^2(f_1, f_2) < 1$. Here $X_1(f_1)$, $X_2(f_2)$ and $X_3(f_3)$ are the Fourier transforms of $x_1(t)$, $x_2(t)$ and $x_3(t)$, respectively. It is convenient to represent contribution of nonlinear coupling from multiple modes to one mode with the summed squared bicoherence $b^2(f) = \sum_{f=f_1\pm f_2} \hat{b}^2(f_1, f_2)$. The bicoherence spectrum and summed squared bicoherence of Mirnov signal are given as Fig. 12. Series of hot spots indicate strong nonlinear interaction and the squared bicoherence reveals that the axisymmetric mode are coupling consequence of two AMs with $(n_{\rm T1}, n_{\rm T2}) = (-1, 1)/(-2, 2)/(-3, 3)$ and $[f_1({\rm kHz}), f_2({\rm kHz})] = (108.5, 128.5)/(98.5, 138.5)/(88.5, 148.5)$. Thus the axisymmetric mode with $n_{\rm E} = n_{\rm T1} + n_{\rm T2} = 0$ and $f_1 + f_2 \approx 237$ kHz is driven by nonlinear couplings of two co-/counter-propagating TAEs. The high-frequency mode $\Omega_{\rm h}(\omega_{\rm h}, \boldsymbol{k}_{\rm h})$ excited by two TAEs, $\Omega_1(\omega_1, \boldsymbol{k}_1)$ and $\Omega_1(\omega_2, \boldsymbol{k}_2)$, with opposite toroidal mode numbers can be investigated by nonlinear gyrokinetic theory.[81] In our experiment, $\omega_1 \simeq \omega_2$ and $n_1 = -n_2$ for the TAEs while the axisymmetric mode with $\omega \approx V_{\rm A}/qR$. The wave number and frequency matching condition during mode coupling process are $\Omega_1(\omega_1, \boldsymbol{k}_1) + \Omega_2(\omega_2, \boldsymbol{k}_2) = \Omega_{\rm h}(\omega_{\rm h}, \boldsymbol{k}_{\rm h})$. For the Ω_1/Ω_2 TAEs, one generally has $|k_{\parallel,1}| = |k_{\parallel,2}| \approx 1/2qR$. Thus, $k_{\parallel,h} = k_{\parallel,1} + k_{\parallel,2} = 0$ or $\pm 1/qR$. For the specific case of the coupling of $m/n = 3/1$ and $-2/-1$ TAEs observed in HL-2A experiments, the nonlinearly generated $\Omega_{\rm h}$ has $m/n = 1/0$. The nonlinearly generated axisymmetric mode is electromagnetic and may not be an EAE because the relative ratio of elongation and inverse aspect ratio is quite small in a circular-cross-section device. A statistical result suggests that amplitudes of the modes are much larger at high field side than low field side, i.e., the mode has an anti-ballooning mode structure. It is found that the axisymmetric mode plays a role of intermediary during coupling process. The $m/n = 1/0$ mode interacts with tearing mode and $n = 0$ mode in the TAE frequency range, then drives series of high frequency sidebands in ellipticity and noncircularity induced Alfvén eigenmode frequency ranges.

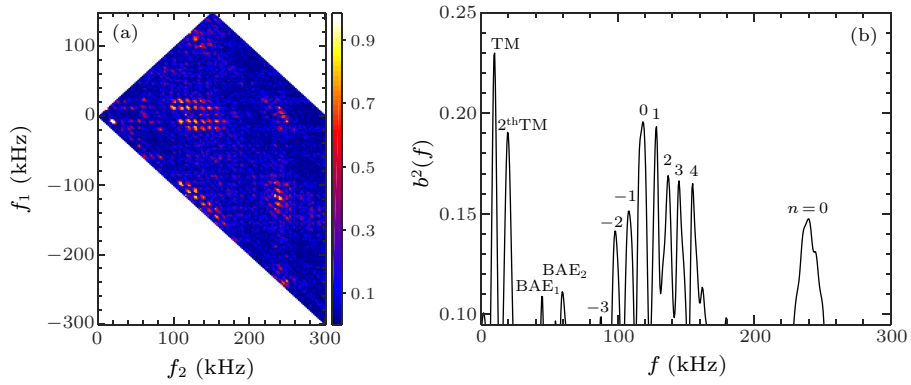

Fig. 12. The squared bicoherence and (b) summed squared bicoherence of Mirnov coil signal for duration of 635–645 ms in low field side. The summed squared bicoherence is limited at 0.08–0.25. Reproduced with permission from Ref. [79]. Copyright 2019 IAEA Vienna.

The nonlinear wave-wave process takes place as well in the presence of energetic electrons.[82] Figure 13 shows the similar nonlinear phenomenon detected by multiple diagnostics at difference positions. The modes lying between two m-BAEs are geodesic acoustic mode induced by energetic particle (EGAM), and can be measured by the 17 GHz (O-mode), 23 GHz (O-mode), and 48 GHz (X-mode) Doppler reflectometers,

but not observed by 34 GHz (X-mode) channel at $\rho = 0.78$, i.e., the EGAM is localized in core plasma. The energy distributions of energetic electrons enhances at different CdTe channels during the appearance of EGAM. The evidence indicates that there are close relationship between the $n = 0$ mode and energetic electrons. Another important feature of EGAM mode on HL-2A is that the mode can only be observed in plasma with line-averaged density $n_e < 0.5\times10^{19}\,\mathrm{m}^{-3}$, whereas the threshold can be improved by auxiliary heating. The EGAM is most probably excited by energetic electrons via three-wave resonance and precessional resonance, i.e., the energetic electrons firstly trigger BAEs via precessional resonance, then EGAM unstable is driven by three-wave resonance among BAEs and tearing mode. Experimental results indicate that an overlap exists between mode radial structures of EGAM and BAEs. Therefore, AEs can propagate poloidally into the region of zonal flow (ZF) due to zonal mode structure of GAM or mode structures overlap, then interact with GAM/ZFs, and finally result in wave energy transfer between the GAM and AEs. Besides the nonlinear couplings of TAE/BAE and $m/n = 2/1$ tearing mode near $q = 2$ rational surface, other multi-scale interactions have also been observed in the HL-2A plasmas, including synchronous linear coupling between $m/n = 1/1$ kink mode and $m/n = 2/1$ tearing mode, nonlinear coupling between AITG/KBM/BAE and $m/n = 1/1$ kink mode near $q = 1$ surface, between $m/n = 1/1$ kink mode and high-frequency turbulence.[83]

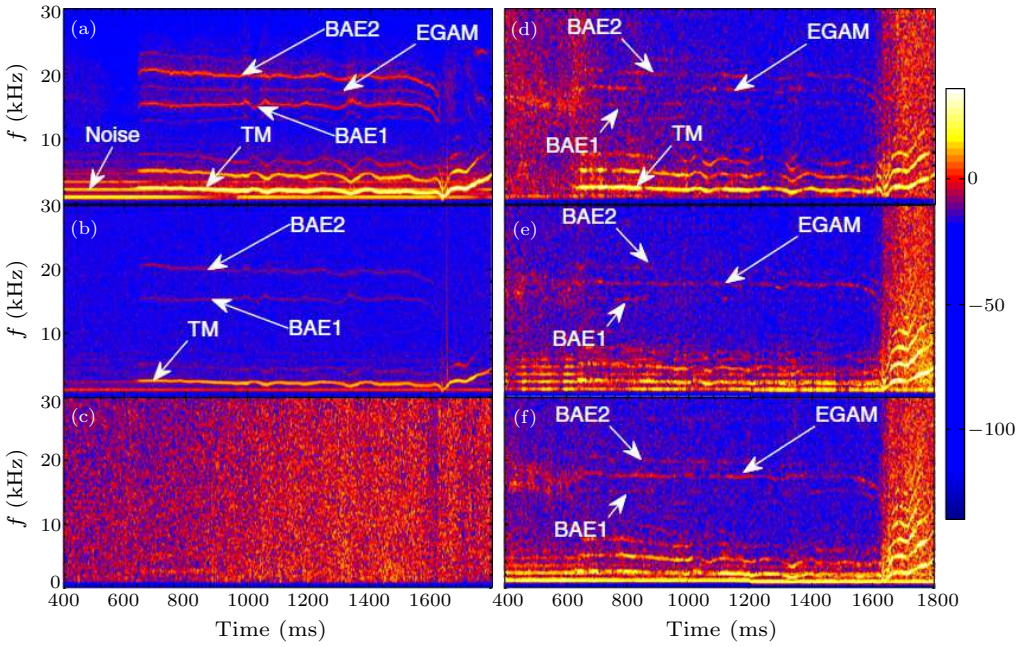

Fig. 13. Spectrograms of (a) Mirnov signal, (b) soft x-ray signal in the core. (c)–(f) Density fluctuations of Doppler reflectometers with different work frequencies: (c) X-mode, $f = 34$ GHz; (d) O-mode, $f = 17$ GHz; (d) O-mode, $f = 23$ GHz; and (f) X-mode, $f = 48$ GHz. Reproduced with permission from Ref. [82]. Copyright 2013 IAEA Vienna.

5. Effects of Alfvénic Modes on Plasma Confinement. Alfvénic modes are driven by energetic particles. In turn, the instability may eject particles from the core plasma and result in abundant fast ions loss, which will degrade EPs confinement and enhance heat loads on the first wall of fusion devices. Those modes can also affect thermal particles in bulk plasma. In this section, experimental effects of Alfvénic modes on energetic and thermal particles confinement are given.

The temporal evolution of fast ion losses due to long-lived mode and sawtooth crashes are measured by a scintillator-based lost fast ion probe,[84] as shown in Fig. 14. The upper panel shows magnetic probe signal and its corresponding spectrogram. The images of fast ion loss distributions at four different intervals are shown in the lower panels. It is found that the long-lived mode leads to loss of fast ions with energy and pitch angle of 32 keV and 67°. The sawtooth seems to cause more serious fast ions losses. The energy covers 27–38 keV while the pitch angle ranges 63°–72°. Fast ions loss may downgrade neutron confinement and the total neutron emission rates are found to drop by 90% during the sawtooth crash. Noted that a new upgrade aimed at improving spatiotemporal resolution is ongoing and the probe will be used to detect the dynamic of fast ions during weak damping Alfvén eigenmodes.

The Alfvénic mode can also interact with thermal particles and enhance energy transport. For example, the RSAEs are found to cause distinct reduction of ion temperature in the core plasma.[85] Figure 15 presents the temporal evolution of electron temperature T_e, ions temperatures T_i at multiple positions, magnetic fluctuation filtered by the numerical filter with frequencies of 65–85 kHz. The electron temper-

atures are modulated by a typical sawtooth activity, but T_i has different trends during a sawtooth period. In the core region, the T_e increases gradually and comes into a flat-top state while T_i goes up firstly and then declines. Because of the poor time resolution of 12.5 ms, three minimums (green prismatics) are artificially added to the ion temperature (×100) at $\rho = 0.04$. Numerical fitting is performed, as shown by the dark curve in Fig. 15(e). Surprisingly, T_i declines immediately when RSAEs are triggered. Noted that the RSAEs are driven by fast ions, but not by thermal ions. It is the high energy tail of thermal ions distribution to enable those particles resonating with RSAEs.

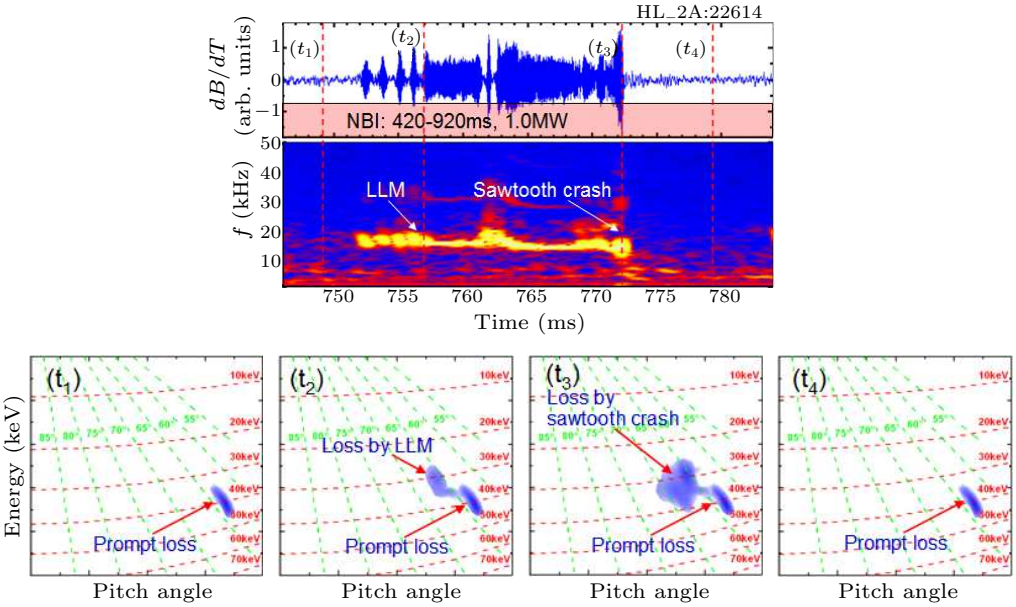

Fig. 14. Typical fast ion losses induced by long-lived mode and sawtooth crash on HL-2A. The upper panel shows the magnetic probe signal and its frequency spectrogram, with frame intervals of the fast ion loss probe demarcated by vertical lines. The fast ion loss distribution images at each time interval are shown in the lower panel. Reproduced with permission from Ref. [84]. Copyright 2015 IAEA Vienna.

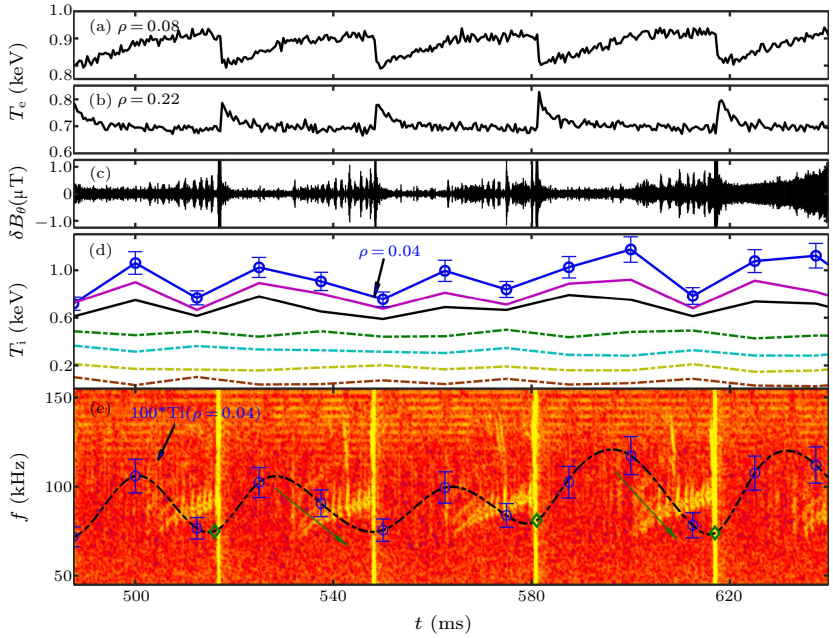

Fig. 15. The temporal electron temperatures detected by ECE radiometer at locations of (a) $\rho = 0.08$ and (b) $\rho = 0.22$. (c) Magnetic signal filtered by the numerical filter with frequencies of 65–85 kHz. (d) Ion temperatures obtained from charge exchange recombination spectroscopy at multiple positions. (e) Spectrogram of Mirnov coil signal for shot 22484, the ion temperature (×100) at $\rho = 0.04$ and the fitting curve are also plotted. Reproduced with permission from Ref. [85]. Copyright 2020 IAEA Vienna.

According to the extended phase space Hamiltonian, one has $\dot{E} = \omega \dot{P}_\phi / n$. Here $\dot{E}$ and $\dot{P}_\phi$ are the derivative of energy and angular momentum, corresponding to heating and transport process, respectively. The ratio of $\frac{\dot{E}/E}{\dot{P}_\phi/P_\phi}$ ranges 0.45–0.64 in this experiment and it means that the angular momentum changes more quickly than energy, i.e., thermal transport plays a dominant role during RSAEs evolution.

To examine the dynamic behavior of thermal transport, ion heat flux perturbation δq_i evaluated by deforming the energy conservation equation for ion perturbation[86,87] is deduced to

$$\delta q_\mathrm{i}(r,t) = -\frac{1}{r}\int_0^r \frac{3}{2} n_\mathrm{i} \frac{\partial \delta T_\mathrm{i}(r,t)}{\partial t} \rho d\rho. \qquad (2)$$

Here, n_i is ion density and assumed as $n_\mathrm{i} = n_\mathrm{e}$, $\delta T_\mathrm{i}(r,t)$ represents ion temperature perturbation induced by RSAEs, in units of keV. The relationship between ion heat flux perturbation at $\rho = 0.04$ normalized by ion density ($\delta q_\mathrm{i}/n_\mathrm{i}$) and amplitude of magnetic fluctuation ($|\delta B_\theta|$) induced by RSAEs is given as Fig. 16. Statistical results suggest that there is a quadratic dependence between thermal ion heat flux perturbation and mode amplitude, which indicates a diffusive mechanism of plasma transport. It should be pointed out that the quadratic fitting curve does not go through zero point, which may imply that there is an amplitude threshold for the heat transport or the pure background thermal ion transport has been added into the RSAEs induced transport.

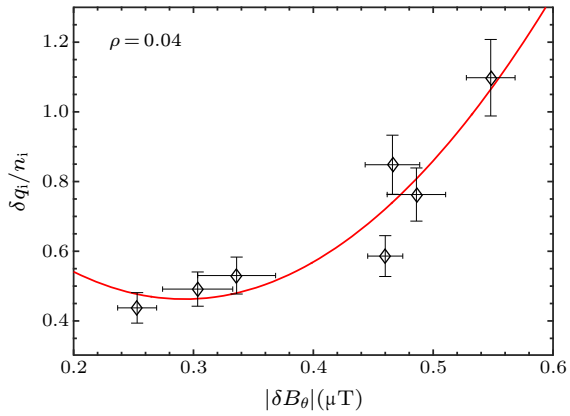

Fig. 16. The relation of ion heat flux perturbation at $\rho = 0.04$ normalized by ion density $\delta q_\mathrm{i}/n_\mathrm{i}$ to amplitude of magnetic fluctuation $|\delta B_\theta|$. The quadratic fitting results have been plotted as the red curve.

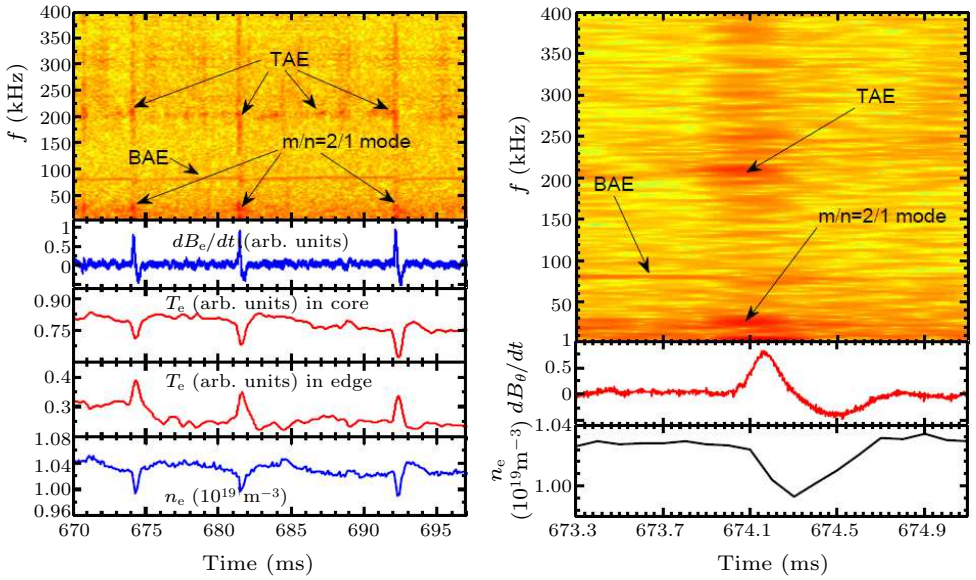

Fig. 17. Avalanche electron heat transport events triggered by nonlinear mode coupling. Mirnov coil signal and corresponding spectrogram, electron temperatures in the edge and core, and line-averaged electron density. Right panels: zoomed-in evolution of the first event shown in the left panels. Reproduced with permission from Ref. [88]. Copyright 2020 IAEA Vienna.

Figure 17 shows another example of electron avalanche event in NBI plasmas.[88] The Mirnov coil signal and its corresponding spectrogram, electron temperatures in the edge and core, and line-averaged electron density are given in the right panels. It is found that when high frequency core-localized TAEs nonlinear couple with low frequency $m/n = 2/1$ fishbone-liked mode, there are several peaks (valleys) on electron temperatures in the core (edge) plasma. Meanwhile, the line-averaged electron density drops by 10% and the magnetic signals are strong disturbed. A detailed investigation of electron temperature fluctuations over a long radial region suggests that the events belong to non-diffusive avalanche electron heat transport processes. The avalanches are extended propagating transport events and usually lead to turbulence spreading or profile relaxation. The phenomenon takes place only when nonlinear mode coupling between TAE and tearing mode occurs on HL-2A tokamak. Though some issues are still question-

able, the experimental evidences can help to understand the generation mechanism of avalanche transport events and shed light on importance of nonlinear multiple mode couplings in physics of plasmas.

6. Suppression of Alfvénic Modes with ECRH. Due to the great effects on plasma confinement, it is urgently necessary to take measures to suppress and control the Alfvénic activity. Three different methods are effective for suppression of Alfvénic modes in the present fusion devices, i.e., three-dimensional magnetic perturbation fields, outboard beam injection and ECRH/ECCD. It is found that magnetic perturbation fields reduce the fast ion drive of modes by depleting resonant fast ions[89] while outboard beam injection suppress the global Alfvén eigenmodes through providing small amounts of beam ions with high pitch angle.[90] However, the physics mechanism is still an enigma though suppression phenomena of Alfvénic mode by ECRH/ECCD have been observed worldwide.[91,92]

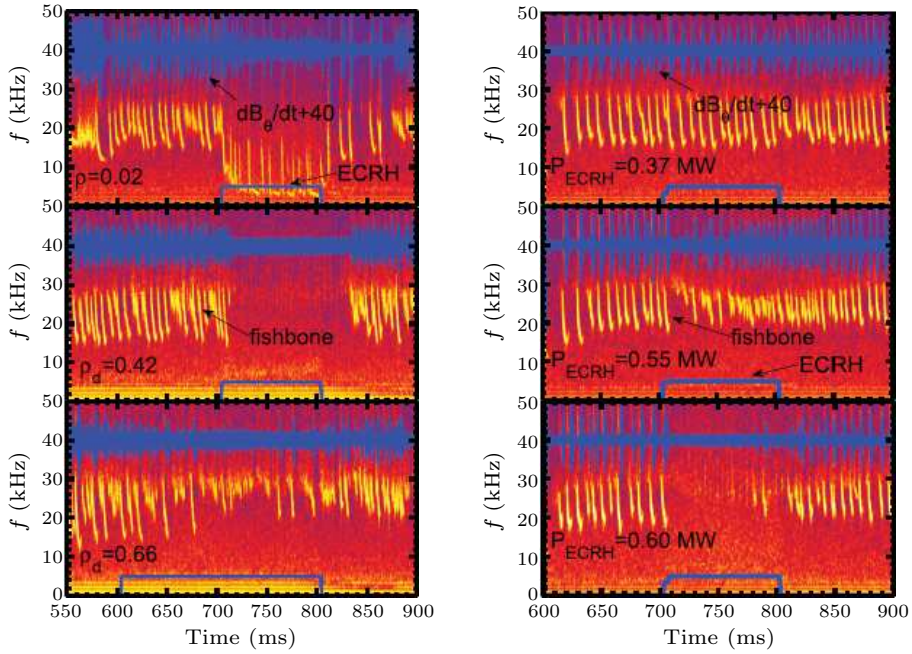

Fig. 18. Effects of ECRH on the stability of ion fishbone activities: with the same ECRH power $P_{\rm ECRH} = 1.0\,{\rm MW}$, but different deposited location (left); for the same deposited location $\rho = 0.42$, but different ECRH power (right). Reproduced with permission from Ref. [93]. Copyright 2018 IAEA Vienna.

Stabilization of internal kink mode by electron cyclotron resonance heating is firstly achieved on HL-2A.[93] The stabilization effect depends on ECRH power and radial deposition location, as shown in Fig. 18. Firstly, the injected powers are set as $P_{\rm ECRH} = 1.0\,{\rm MW}$ and the electron cyclotron waves are launched to location of $\rho = 0.02$, 0.42 and 0.66. The best suppression effect appears in $\rho = 0.42$. Then, the radial deposition location of ERCH is arranged at $\rho = 0.42$ and the $P_{\rm ECRH}$ scans from 0.37 WM to 0.6 MW. The suppress effect becomes better when power increases and the fishbone activities are expected to be completely suppressed when the power exceeds a certain threshold. To reveal the underlying mechanism, the internal kink mode dispersion relation in the presence of trapped fast ions and resistive effect is numerically solved with experimental data. The growth rate and real frequency mode decrease when fast ions beta increases, which indicates that resistivity becomes more important and reveals the resistive nature of fishbone modes. The growth rate falls down but the real frequency rises with increasing magnetic Reynolds number and it means that the strongly unstable resistive mode converts into a weakly general fishbone mode. The numeral results, which are confirmed by NIMROD simulation,[94] can well explain the observation and provide a possible mechanism of Alfvénic mode suppression, i.e., ECRH weakens mode growth rate and enhances the critical fast ion beta by varying magnetic Reynolds number. ECRH can also mitigate long-lived modes via changing magnetic shear in the mode location.[95]

7. Conclusions. Amount of Alfvénic modes, which may determine plasma confinement and transport properties in ITER and CFETR, are driven by energetic particles on HL-2A tokamak. Those modes show different responses to nonlinear wave-particle and wave-wave resonances, and affect plasma confinement via multiple routes. In addition, attention is also paid to active control technology of EPs driven instability. Those crucial experimental results have been summarized in this review and more details can be found in the references listed in Table 2.

Table 2. Alfvénic activities on the HL-2A tokamak.

Title	Driven by fast ions	Driven by fast electrons
TAE	Refs. [27,77,79,88]	Ref. [31]
RSAE	Refs. [33,85]	
BAE	Ref. [40]	Refs. [41,43]
AITG/KBM	Refs. [47,51,52]	
Fishbone	Refs. [53,58,93]	Refs. [55,56]
EGAM		Ref. [82]

Especially, the following achievements may greatly contribute to better understanding of energetic particle physics in future burning plasmas.

(1) The first evidences of e-BAE and non-resonant e-fishbone modes enrich knowledge of wave-particle interaction. Those modes can be utilized to simulate and analyze the analogous effect of alpha particles characterized by small dimensionless orbits similar to energetic electrons in tokamak plasmas.

(2) The new findings of $m/n = 2/1$ fishbone modes shed light on understanding of tearing mode induced energetic particle loss and particle acceleration during magnetic reconnection in laboratory or space plasmas.

(3) Three kinds of axisymmetric modes in BAE, TAE and EAE frequency regions are driven by nonlinear coupling among Alfvénic modes and tearing mode. Those axisymmetric modes may be an energy channeling between macro-, meso- and micro-scale. Further, the nonlinear couplings induce energy transfer among TMs, AEs and $n = 0$ modes. It could be one of mechanisms of energy cascade in the Alfvén turbulence.

(4) Effects of Alfvénic modes on thermal confinements, including ion heat transport induced by RSAEs and electrons avalanche event triggered by nonlinear mode coupling, have been newly observed. This will help to better understand the energy or particle transport induced by energetic ions driven instabilities.

(5) The first achievement of stabilization of fishbone activity with ECRH will provide technology basis for suppression and control of EPs driven instability in fusion devices.

In the future, experimental campaign related to energetic particle physics on HL-2A/2M will be devoted to the current research hot spots,[96] such as fast ions losses induced by SAWs fluctuations and active control of Alfvénic modes. Those experiments will be performed in the high normalized beta plasma, especially on HL-2M, which are developed for the fundamental research of physics for advanced plasma scenarios with high beta, high elongation, high triangularity, snowflake and super-X divertors, and achieve first operation in 2020. To monitor the dynamic evolution of EPs, more advanced diagnostics are needed. For example, the FIDA is a powerful tool to detect fast ions distributions, which are crucial for particle losses and transports, and two-dimensional FIDA imaging technologies enable overview of fast ions.[97,98] The collective Thomson scattering has potential for mapping out fast ion phase space distribution by providing spatially localized measurements of ion velocity distribution with energies into MeV range.[99] Those energetic particle diagnostics will and should be developed, especially for HL-2M with NBI and ECRH power reaching at 10 MW and 20 MW, respectively. While suppression effects of ECRH have been found on fishbone instability, more experiments should be carried out. On the one hand, the ECRH should be used to control other Alfvén eigenmodes, especially the weak damping modes with spacial overlapped structure. On the other hand, more technologies, such as three-dimensional magnetic perturbation fields, should be explored in the future. Combination of multiple methods may optimize the suppress and control effect even though it is much complicated. Finally, the experimental verification should closely combine with numerical simulations and analytical theory, which will enhance the predictive ability of present achievements for future burning plasma scenarios.

References

[1] Zonca F *et al.* 2015 *Plasma Phys. Control. Fusion* **57** 014024
[2] Chen L and Zonca F 2016 *Rev. Mod. Phys.* **88** 015008
[3] Gorelenkov N N *et al.* 2014 *Nucl. Fusion* **54** 125001
[4] Heidbrink W W and White R B 2020 *Phys. Plasmas* **27** 030901
[5] García-Muñoz M *et al.* 2010 *Phys. Rev. Lett.* **104** 185002
[6] Chen X *et al.* 2013 *Phys. Rev. Lett.* **110** 065004
[7] Heidbrink W W *et al.* 2007 *Phys. Rev. Lett.* **99** 245002
[8] Nazikian R *et al.* 2006 *Phys. Rev. Lett.* **96** 105006
[9] Kolesnichenko Y I *et al.* 2020 *Nucl. Fusion* **60** 112006
[10] Stutman D *et al.* 2009 *Phys. Rev. Lett.* **102** 115002
[11] Kolesnichenko Y I *et al.* 2010 *Phys. Rev. Lett.* **104** 075001
[12] Fasoli A *et al.* 2002 *Plasma Phys. Control. Fusion* **44** B159
[13] Fisch N J and Herrmann M 1994 *Nucl. Fusion* **34** 1541
[14] Sasaki M *et al.* 2011 *Plasma Phys. Control. Fusion* **53** 085017
[15] Wong K L *et al.* 2004 *Phys. Rev. Lett.* **93** 085002
[16] Sharapov S E *et al.* 2006 *Nucl. Fusion* **46** S868
[17] Wei Y L *et al.* 2014 *Rev. Sci. Instrum.* **85** 103503
[18] Shi Z B *et al.* 2014 *Rev. Sci. Instrum.* **85** 023510
[19] Zhong W L *et al.* 2014 *Rev. Sci. Instrum.* **85** 013507
[20] Shi P W *et al.* 2016 *Plasma Sci. Technol.* **18** 708
[21] Shi Z B *et al.* 2018 *Rev. Sci. Instrum.* **89** 10H104
[22] Jiang M *et al.* 2013 *Rev. Sci. Instrum.* **84** 113501
[23] Yang Q W *et al.* 2014 *Rev. Sci. Instrum.* **85** 11D857
[24] Zonca F and Chen L 2014 *Phys. Plasmas* **21** 072121
[25] Cheng C Z *et al.* 1985 *Ann. Phys.* **161** 21
[26] Wong K L *et al.* 1991 *Phys. Rev. Lett.* **66** 1874
[27] Shi P W *et al.* 2017 *Phys. Plasmas* **24** 042509
[28] Berk H L *et al.* 1992 *Phys. Lett. A* **162** 475
[29] Tsai S and Chen L 1993 *Phys. Fluids B* **5** 3284
[30] Fu G Y and Cheng C Z 1992 *Phys. Fluids B* **4** 3722
[31] Yu L M *et al.* 2018 *Phys. Plasmas* **25** 012112
[32] Wang J L *et al.* 2020 *Nucl. Fusion* **60** 112012
[33] Chen W *et al.* 2014 *Nucl. Fusion* **54** 104002
[34] Berk H L *et al.* 2001 *Phys. Rev. Lett.* **87** 185002
[35] Edlund E M *et al.* 2009 *Phys. Rev. Lett.* **102** 165003
[36] Van Zeeland M A *et al.* 2016 *Nucl. Fusion* **56** 112007
[37] Breizman B N *et al.* 2011 *Plasma Phys. Control. Fusion* **53** 054001
[38] Yang Y R *et al.* 2020 *Nucl. Fusion* **60** 106012
[39] Heidbrink W W *et al.* 1993 *Phys. Rev. Lett.* **71** 855
[40] Shi P W *et al.* 2019 *Nucl. Fusion* **59** 066015
[41] Chen W *et al.* 2010 *Phys. Rev. Lett.* **105** 185004
[42] Buratti P *et al.* 2005 *Nucl. Fusion* **45** 1446
[43] Chen W *et al.* 2010 *J. Phys. Soc. Jpn.* **79** 044501
[44] Biancalani A *et al.* 2010 *Phys. Rev. Lett.* **105** 095002

[45] Hirose A and Elia M 1996 *Phys. Rev. Lett.* **76** 628
[46] Biglari H and Chen L 1991 *Phys. Rev. Lett.* **67** 3681
[47] Chen W *et al.* 2016 *Nucl. Fusion* **56** 036018
[48] Zonca F *et al.* 1999 *Phys. Plasmas* **6** 1917
[49] Zonca F *et al.* 1996 *Plasma Phys. Control. Fusion* **38** 2011
[50] Zonca F *et al.* 1998 *Plasma Phys. Control. Fusion* **40** 2009
[51] Chen W *et al.* 2018 *Nucl. Fusion* **58** 056004
[52] Chen W *et al.* 2016 *Europhys. Lett.* **116** 45003
[53] Chen W *et al.* 2010 *Nucl. Fusion* **50** 084008
[54] Gryaznevich M P *et al.* 2008 *Nucl. Fusion* **48** 084003
[55] Yu L M *et al.* 2013 *Nucl. Fusion* **53** 053002
[56] Yu L M *et al.* 2017 *Nucl. Fusion* **57** 036023
[57] Zonca F *et al.* 2007 *Nucl. Fusion* **47** 1588
[58] Chen W *et al.* 2019 *Nucl. Fusion* **59** 096037
[59] Zhu X L *et al.* 2020 *Nucl. Fusion* **60** 046023
[60] Chen L and Zonca F 2013 *Phys. Plasmas* **20** 055402
[61] Berk H L and Breizman B N 1990 *Phys. Fluids B* **2** 2246
[62] Chen L *et al.* 1984 *Phys. Rev. Lett.* **52** 1122
[63] Zonca F *et al.* 2015 *New J. Phys.* **17** 013052
[64] Hahm T S and Chen L 1995 *Phys. Rev. Lett.* **74** 266
[65] Zonca F *et al.* 1995 *Phys. Rev. Lett.* **74** 698
[66] Chen L and Zonca F 2012 *Phys. Rev. Lett.* **109** 145002
[67] Qiu Z *et al.* 2018 *Phys. Rev. Lett.* **120** 135001
[68] Berk H L *et al.* 1997 *Phys. Lett. A* **234** 213
[69] Zhu J *et al.* 2014 *Nucl. Fusion* **54** 123020
[70] Osakabe M *et al.* 2006 *Nucl. Fusion* **46** S911
[71] Berk H L *et al.* 1996 *Phys. Rev. Lett.* **76** 1256
[72] Heeter R F *et al.* 2000 *Phys. Rev. Lett.* **85** 3177
[73] Lilley M K *et al.* 2009 *Phys. Rev. Lett.* **102** 195003
[74] Hou Y M *et al.* 2018 *Nucl. Fusion* **58** 096028
[75] Zonca F and Chen L 1999 *The 6th IAEA TCM on Energetic Particles in Magnetic Confinement Systems* (Jaeri, Naka, Japan 12–14 October 1999)
[76] Crocker N A *et al.* 2006 *Phys. Rev. Lett.* **97** 045002
[77] Chen W *et al.* 2014 *Europhys. Lett.* **107** 25001
[78] Diallo A *et al.* 2018 *Phys. Rev. Lett.* **121** 235001
[79] Shi P W *et al.* 2019 *Nucl. Fusion* **59** 086001
[80] Kim Y C and Powers E J 1979 *IEEE Trans. Plasma Sci.* **7** 120
[81] Wei S Z *et al.* 2019 *Phys. Plasmas* **26** 074501
[82] Chen W *et al.* 2013 *Nucl. Fusion* **53** 113010
[83] Chen W *et al.* 2017 *Nucl. Fusion* **57** 114003
[84] Zhang Y P *et al.* 2015 *Nucl. Fusion* **55** 113024
[85] Shi P W *et al.* 2020 *Nucl. Fusion* **60** 064001
[86] Tamura N *et al.* 2005 *Phys. Plasmas* **12** 110705
[87] Lopes C N J 1995 *Plasma Phys. Control. Fusion* **37** 799
[88] Chen W *et al.* 2020 *Nucl. Fusion* **60** 094003
[89] Bortolon A *et al.* 2013 *Phys. Rev. Lett.* **110** 265008
[90] Fredrickson E D *et al.* 2017 *Phys. Rev. Lett.* **118** 265001
[91] Maslovsky D *et al.* 2003 *Phys. Rev. Lett.* **90** 185001
[92] Nagaoka K *et al.* 2013 *Nucl. Fusion* **53** 072004
[93] Chen W *et al.* 2018 *Nucl. Fusion* **58** 014001
[94] Yang Y R *et al.* 2019 *Plasma Sci. Technol.* **21** 085101
[95] Wei D *et al.* 2014 *Nucl. Fusion* **54** 013010
[96] Chen W *et al.* 2020 *Chin. Phys. Lett.* **37** 125001
[97] Van Zeeland M A *et al.* 2009 *Plasma Phys. Control. Fusion* **51** 055001
[98] Van Zeeland M A *et al.* 2010 *Plasma Phys. Control. Fusion* **52** 045006
[99] Bindslev H *et al.* 1999 *Phys. Rev. Lett.* **83** 3206